Bull. Mater. Sci., Vol. 35, No. 3, June 2012, pp. 347–352. © Indian Academy of Sciences.

ZnO–TiO_2 nanocomposite: Characterization and moisture sensing studies

N K PANDEY*, K TIWARI and AKASH ROY
Department of Physics, University of Lucknow, Lucknow 226 007, India

MS received 11 January 2011; revised 14 August 2011

Abstract. **This paper reports morphological and relative humidity sensing behaviour of ZnO–TiO_2 nanocomposite powder pellets obtained through solid-state reaction route. Resistance of the pellets is observed to decrease with increase in relative humidity in the 10–90% range. Sensing element with 15 wt % of TiO_2 in ZnO shows best results with a sensitivity of 9·08 MΩ/%RH in 10–90% relative humidity range. This sensing element manifests crystallite size of 71 nm as measured from XRD and average grain size of 207 nm calculated from SEM micrograph. This sensing element manifests low hysteresis, less effect of ageing and good reproducibility. Response and recovery times of this sensing element are measured to be 84 s and 396 s, respectively.**

Keywords. **Sensor; humidity; TiO_2; ZnO; XRD; SEM.**

1. Introduction

Research has been going on to find suitable materials that show good sensitivity over large range of relative humidity (RH), low hysteresis and properties that are stable to thermal cycling and exposure to the various chemicals likely to be present in the environment. Ceramic humidity sensors, particularly those based on porous and sintered metal oxides have been attracting attention due to their chemical and physical stability and mechanical strength (Traversa 1995; Yarkin 2003). ZnO is an attractive semiconductor oxide having a wide bandgap and is known for its *n*-type conduction due to the presence of oxygen vacancies (Kishimoto *et al* 2006; Yogeeswaran *et al* 2006). Doped ZnO or ZnO mixed with other oxides exhibit various properties, different types of morphologies and have many applications (Jayanti *et al* 2009). TiO_2 is one of the most extensively studied metal oxides because of its remarkable optical and electrical properties.

Ivetic *et al* (2007) reported results with composition of ZnO and SnO_2 powders with a molar ratio of 2:1 and discussed photo acoustic investigation of thermal and transport properties of bulk zinc stannate synthesized by the reaction sintering method. Raid *et al* (2006) reported results with dopants of 1, 2 and 3% weight of (Al, Cu, I) powder with ZnO and discussed microstructural, optical and electrical properties of ZnO by chemical spray pyrolysis. Yavale *et al* (2007) studied the effect of humidity on pure and doped SnO_2 and ZnO thick films. Margionte *et al* (2006) reported results with compositions of 0·5 and 1% mol of WO_3 and 1 and 2% mol of ZnO powder with SnO_2 and discussed their microstructural, ohmic characteristic and densification. Yildiz *et al* (2007) reported results of ZnO–TiO_2 compositions having 1, 2, 3 and 4% weight of TiO_2 powder in ZnO and discussed their microstructure properties and densification. Morphological and humidity sensing studies of pure ZnO (Pandey and Tiwari 2010), ZnO–Cu_2O nanocomposite (Pandey *et al* 2009, 2011), ZnO–WO_3 nanocomposite (Pandey *et al* 2008) and ZnO–WO_3–TiO_2 nanocomposite (Pandey *et al* 2009) have been reported. This paper presents morphological and humidity sensing studies of ZnO–TiO_2 nanocomposites prepared by solid state reaction route. The sensitivity in the case of ZnO–TiO_2 nanocomposite is lower (9·08 MΩ/%RH) than the sensing element of pure ZnO (12·89 MΩ/%RH) but is nearly two fold as compared to the sensing element of ZnO–Cu_2O nanocomposite (4·78 MΩ/%RH). The response and recovery times in the case of ZnO–TiO_2 nanocomposite (84 s, 396 s) are lower than that of sensing element of pure ZnO (128 s, 452 s) but higher than that of ZnO–Cu_2O nanocomposite (76 s, 196 s). The repeatability (±0·33%) in the case of ZnO–TiO_2 nanocomposite sensing element is much higher than that of the sensing element of pure ZnO (±2·80%) and also that of ZnO–Cu_2O nanocomposite (±0·63%). Similarly, the hysteresis is much lower for ZnO–TiO_2 nanocomposite sensing element (1·90%) as compared to the sensing element of pure ZnO (2·80%) and ZnO–Cu_2O nanocomposite (2·30%). Thus, on addition of TiO_2 in ZnO, there is improvement in the sensor performance in terms of repeatability and hysteresis with some trade off in terms of sensitivity.

2. Sample preparation and experimental

10, 15 and 20% weight of TiO_2 powder (Qualigens, 99·9% pure) in ZnO (Qualigens, 99·9% pure) were mixed

*Author for correspondence (nkp1371965@gmail.com)

uniformly for 30 min. 10% weight of glass powder was added as binder to increase strength of the sample. The powders were pressed in pellet shape by uniaxially applying a pressure of 260 MPa in hydraulic press machine at room temperature. Samples were labelled *S*-10, *S*-15 and *S*-20, respectively. Samples had a diameter of 8 mm and thickness, 4 mm. The samples were annealed in air at temperatures of 300°C, 400°C and 500°C for 3 h in electric muffle furnace (Ambassador, India). Pellet samples of pure ZnO with same dimensions were prepared by the same method for reference and comparison. This sample was labelled *S*-0.

The nature of the studies undertaken here was two-fold. On the one hand, morphological and crystalline structures were studied for different compositions of ZnO and TiO_2 and, on the other hand, changes in response to humidity were investigated. Scanning electron microscopy (SEM) was used to investigate the morphological changes. The study of surface morphology of sensing elements was carried out using scanning electron microscope (LEO-430, Cambridge, England). X-ray diffraction (XRD) was used to look into the crystalline structure. X-ray diffraction was studied using XPERT PRO-Analytical XRD system (The Netherlands). The wavelength of the Cu-Kα radiation used was 1·54060 Å. Finally, humidity sensing studies of different compositions of ZnO and TiO_2 were investigated.

After sintering, samples were exposed to humidity in a humidity control chamber. Inside the humidity chamber, a thermometer (±1°C) and standard hygrometer (Huger, Germany, ±1 % RH) were placed for the purpose of calibration. Variation in resistance was recorded with change in relative humidity at room temperature (27°C). Relative humidity was measured using the standard hygrometer. Variation in resistance of the pellet was recorded using a resistance meter (sino meter: a multimeter, ±0·001 MΩ, model: VC-9808). Copper electrode was used to measure resistance of the pellet. The resistance of the pellet was measured normal to the cylindrical surface of the pellet. The electrical resistance of the sensing element in the form of pellet was determined by a two-probe method at different relative humidity levels. The electrical contacts were made on the surface of pellet by means of two thin copper sheets. Given the high resistivity of the materials under consideration, the potential inaccuracy due to contact resistance was assumed to be negligible. The surface contact area of all the sensing elements with the electrodes was 113·11 mm^2 and the cylindrical surface area that was exposed to humidity in the chamber was also 113·11 mm^2. These values were kept constant for all the sensing elements. The experimental sample was electrically connected to a power supply and sino meter (VC 9808) in series. After studying humidity sensing properties, sensing elements were kept in laboratory environment and their humidity sensing characteristics regularly monitored. To see the effect of ageing, the sensing properties of these elements have been examined again in the humidity control chamber after six months. The stability of the sensing elements was checked by keeping the sensing element at fixed values of % RH in the chamber and the values of resistance recorded as a function of time. The values were found to be stable within ±3% of the measured values.

3. Results and discussion

We have demonstrated the feasibility of the nanocomposites of porous metal oxides, prepared by solid state reaction route, as humidity sensor. The performance characteristics, such as sensitivity, reproducibility and response time, have been recorded and correlated to its microstructures. Here it has been shown that humidity sensor can be made from the binary system of ZnO–TiO_2 nanocomposite.

3.1 *Humidification process*

Figure 1 shows graphs between resistance of the sensing elements with the change in relative humidity (% RH); **a**, **b** and **c** are the curves for the sensing elements *S*-10, *S*-15 and *S*-20, respectively. We observe continuous decrease in the value of resistance of all the sensing elements with increase in % RH. The phenomenon of decrease in resistance may be explained by the process of Grotthuss chain reaction (Yadav *et al* 2007).

ZnO and TiO_2 both are *n*-type semiconductors; hence, sensitivity to humidity is a result of electronic conduction (Ohbuchi *et al* 2001; Lopatiuk and Chernyak 2005). As semiconducting dry oxides of ZnO–TiO_2 nanocomposite are brought in contact with humid air, water molecules chemisorb on the available sites of the oxide surface. The adsorption of water molecules on the surface takes place via a dissociative chemisorption process which may be described in a two-step process as given here: (i) Water molecules

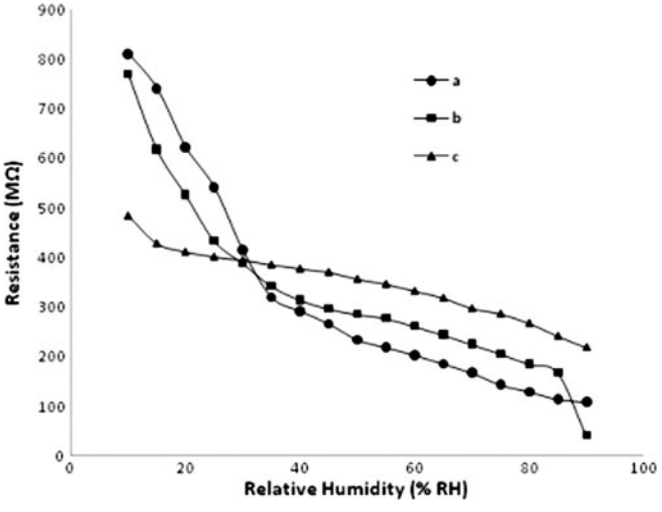

Figure 1. Humidification graphs: Variation of resistance with % RH for sensing elements *S*-10, *S*-15 and *S*-20 for annealing temperature, 500°C, for the relative humidity range 10–90% RH. a. sensing element, *S*-10; b. sensing element, *S*-15 and c. sensing element, *S*-20.

adsorbed on grain surface reacts with the lattice, A ($A \rightarrow$ Zn or Ti) as

$$H_2O + O_o + A \leftrightarrow 2OH - A + V_o + 2e^-, \quad (1)$$

here O_o is the lattice oxygen and V_o the vacancy created at the oxygen site according to the reaction:

$$O_o \leftrightarrow O^{2-} + V_o. \quad (2)$$

(ii) Doubly ionized oxygen, displaced from the lattice, reacts with H^+ coming from the dissociation of water molecules to form a hydroxyl group as given below:

$$H^+ + O^{2-} \leftrightarrow OH^-. \quad (3)$$

ZnO and TiO_2 both have electron vacancies. Hence, because of this reaction, the electrons are accumulated at the ZnO/TiO_2 surface and consequently, the resistance of the sensing element decreases with increase in relative humidity.

Three compounds may exist in ZnO–TiO_2 system viz. Zn_2TiO_4 (cubic), $ZnTiO_3$ (hexagonal) and $Zn_2Ti_3O_8$ (cubic) (Dulin and Rase 1960; Reddy *et al* 1984). Due to superior electrical properties, ilmenite-type hexagonal $ZnTiO_3$ compound possibly plays a dominant role in the present sensor operation where a decrease in the value of resistance is observed with increase in % relative humidity (Huang *et al* 2001; Xia *et al* 2003).

All graphs in figure 1 show that from 10 to 40% RH there is a rapid change in resistance while in 40 to 90% RH range the fall in resistance is slow; it indicates that in 10 to 40% RH range sensitivity of the sample is high whereas in 40 to 90% RH range sensitivity is low. It is understood that the increase in conductivity of the sample with relative humidity in the lower range (<40% RH) is due to the adsorption of water molecules on the pellet surface with capillary nanopores. Higher porosity increases surface to volume ratio of the materials and enhances diffusion rate of water into or out-off the porous structure; and thus, helps in getting good sensitivity. At high relative humidity (>40% RH), liquid water condenses in the capillary like pores, forming a liquid like layer. Depending on the microstructures like distribution of porosity, network of pores (that are expected to provide sites for humidity adsorption), etc the change in slope around 40% RH may be different for different sensing elements and also for different annealing temperatures. This leads to cross over of the graphs. It is very difficult to pinpoint the exact reason for the cross-over. This behaviour is quite often observed in the humidity sensing exercise by the metal oxide sensing elements.

Sensitivity of humidity sensor is defined as the change in resistance (ΔR) of sensing element per unit change in relative humidity (RH %). For calculation of sensitivity, the humidity from 10 to 90% RH has been divided in equal intervals of 5% RH each. Difference in the value of the resistance for each of this interval has been calculated and then divided by 5. The average has been taken for all these calculated values. Formula for calculation of sensitivity of the sensing elements may be written as given below:

$$\text{Sensitivity} = (\Delta R) / (\Delta\%\text{RH}). \quad (4)$$

Values of sensitivity calculated for sensing elements *S*-10, *S*-15 and *S*-20 for annealing temperatures of 300°C, 400°C and 500°C are shown in table 1. Column **a** in table 1 represents values of sensitivity for increasing cycle of relative humidity (humidification). It can be seen from table 1 that the sensing element of pure ZnO (*S*-0) shows higher values of sensitivity. Of the ZnO–TiO_2 system sensing element *S*-15 annealed at 500°C shows the value of maximum sensitivity of 9·08 MΩ/%RH.

3.2 *Humidification and desiccation processes (hysteresis effect)*

Metal oxides and binary systems of metal oxides show deviation in their behaviour in the decreasing cycle of % RH from those in increasing cycle of % RH. Minimization of this hysteresis behaviour is an important condition for sensor application. To determine the hysteresis effect in the ZnO–TiO_2 sensing elements annealed at 500°C, the humidity in the chamber has been increased from 10% RH to 90% RH and then cycled down to 10% RH. Variation of resistance of the sensing elements has been recorded both for increasing and decreasing cycles of % RH for all sensing elements *S*-10, *S*-15 and *S*-20 for annealing temperatures of 300°C, 400°C and 500°C. All the sensing elements manifest hysteresis for all the annealing temperatures. For the

Table 1. Values of sensitivity for sensing elements *S*-0, *S*-10, *S*-15 and *S*-20 for different annealing temperatures in range of relative humidity from 10 to 90 % RH. a. increasing cycle of % RH; b. decreasing cycle of % RH; c. increasing cycle of % RH after six months.

Annealing temperatures	Sensitivity (MΩ/%RH) of sensing elements											
	S-0			*S*-10			*S*-15			*S*-20		
	a	*b*	*c*	*a*	*b*	*c*	*a*	*b*	*c*	*a*	*b*	*c*
300°C	10·26	9·78	10·23	8·00	6·76	7·38	8·76	8·46	6·94	3·33	3·46	3·76
400°C	11·13	10·25	10·25	8·12	6·61	7·42	8·91	8·83	8·00	4·18	4·26	4·01
500°C	12·89	13·25	13·25	7·78	7·46	7·68	9·08	8·78	9·11	6·19	6·66	4·96

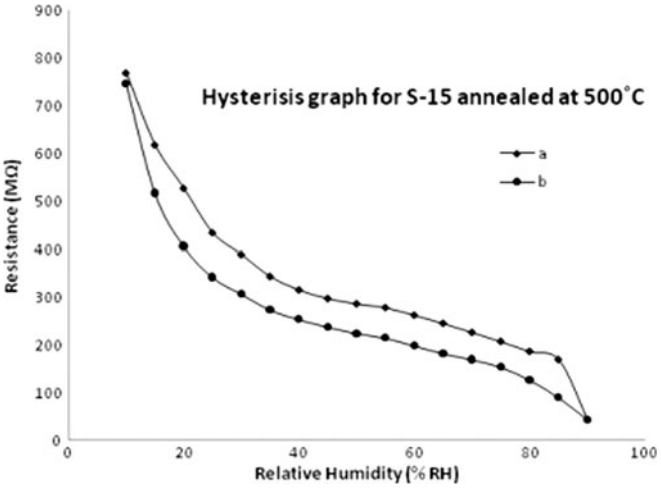

Figure 2. Variation of resistance with change in % RH for sensing element *S*-15 for annealing temperature, 500°C, for the relative humidity range 10–90% RH; a. humidification process and b. desiccation process.

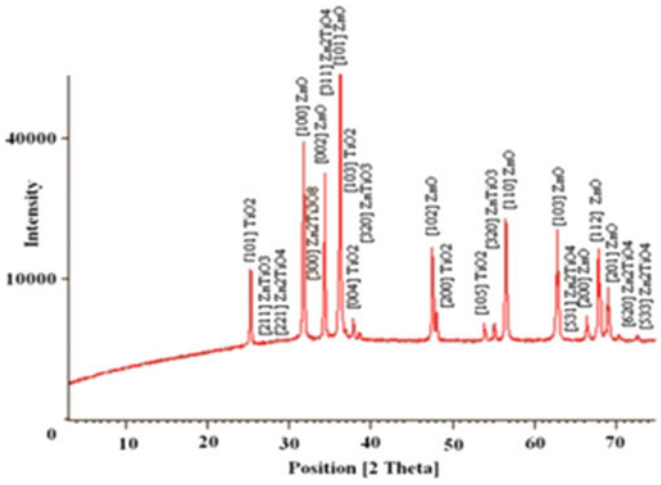

Figure 3. XRD pattern for sensing element *S*-15 for annealing temperature, 500°C.

annealing temperature of 500°C, it has been observed that all the sensing elements show lower hysteresis. In figure 2 we present variation of resistance with % RH of the sensing element *S*-15 of the ZnO–TiO_2 systems for annealing temperature of 500°C. Graph **a** in figure 2 is for increasing cycle of % RH and graph b is for decreasing cycle of % RH. Column **b** in table 1 depicts values of sensitivity for decreasing cycle of % RH.

The phenomenon of hysteresis may be attributed to the initial chemisorptions on the surface of the sensing elements. This chemisorbed layer once formed is not further affected by exposure to or removal of humidity, it can be thermally desorbed only. Hence in the decreasing cycle of % RH, the initially adsorbed water is not removed fully leading to hysteresis. It has been observed that all sensing elements have acceptable hysteresis values; sample *S*-10 has a hysteresis of 4·11%, sample *S*-15 has a hysteresis of 1·90% and sample *S*-20 has a hysteresis of 7·59% for annealing temperature of 500°C. The value of sensitivity for the sensing element of pure ZnO for the annealing temperature of 500°C is 12·89 MΩ/%RH as compared to 9·08 MΩ/%RH for *S*-15. However, for the same annealing temperature of 500°C, the value of hysteresis is high at 2·80% for the sensing element of pure ZnO as compared to *S*-15 where it is 1·90% (Pandey and Tiwari 2010). The data sheets of some commercially available humidity sensors have indicated hysteresis values in the range from 1·20–5·00% (Thermoset Polymer-based Capacitive Sensors - HIH-3605 humidity sensor data sheet). Our best sensing element *S*-15 has shown small value of hysteresis of 1·90%.

3.3 *X-ray diffraction analysis*

Figure 3 shows X-ray pattern for the sensing element *S*-15 annealed at 500°C. The pattern shows extent of crystallization of the sensing element in the form of powder. The average crystalline size of the samples has been calculated using Scherrer's formula

$$D = K\lambda / B\cos\theta. \tag{5}$$

Here, D is the crystallite size, K a fixed number of 0·9, λ the X-ray wavelength, θ the Bragg angle and B the full width at half maximum of the peak. The average crystallite size measured for sensing elements *S*-0, *S*-10, *S*-15 and *S*-20 are 59 nm, 89 nm, 71 nm and 80 nm, respectively. XRD pattern shows peaks of ZnO–TiO_2 binary system. In addition to these peaks, the pattern also manifests presence of peaks of cubic Zn_2TiO_4 (zinc orthotitanate), cubic $Zn_2Ti_3O_8$ and hexagonal $ZnTiO_3$ formed due to solid state reaction between TiO_2 and ZnO.

3.4 *Scanning electron microscope (SEM) study*

In figure 4 we present SEM micrograph of the nanocomposite of the sensing element *S*-15 annealed at a temperature of 500°C. SEM micrograph shows flakes of TiO_2 scattered throughout ZnO substrate forming a network of pores that are expected to provide sites for humidity adsorption. It has been observed that the grain density was getting increased with increase in the % weight of TiO_2 in ZnO. It seems as if the grain size of ZnO were getting inhibited with increasing composition of TiO_2. The average grain size for the sensing elements *S*-0, *S*-10, *S*-15 and *S*-20 calculated from SEM micrographs are 236 nm, 300 nm, 207 nm and 236 nm, respectively. Here, we observe that in the ZnO–TiO_2 systems, both the crystallite size and grain size are the minimum for sensing element *S*-15. SEM micrographs show that the sensing elements manifest porous structure. An observation of the crystallite size and grain size would suggest that smaller crystallites are getting agglomerated to form larger grains. In this process, more of the surface areas of

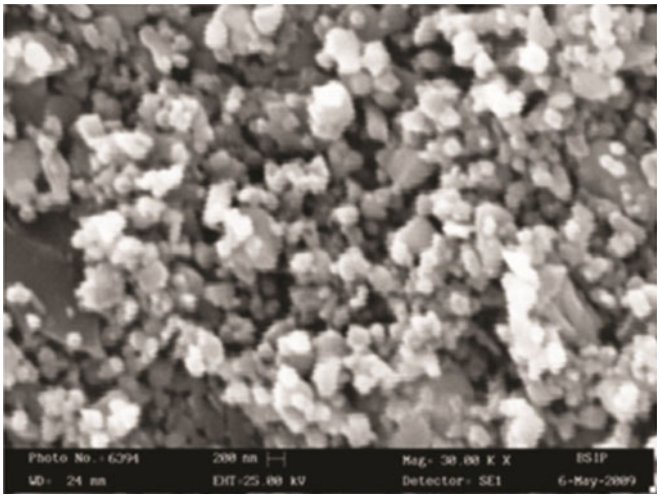

Figure 4. SEM micrograph for sensing element *S*-15 for annealing temperature, 500°C.

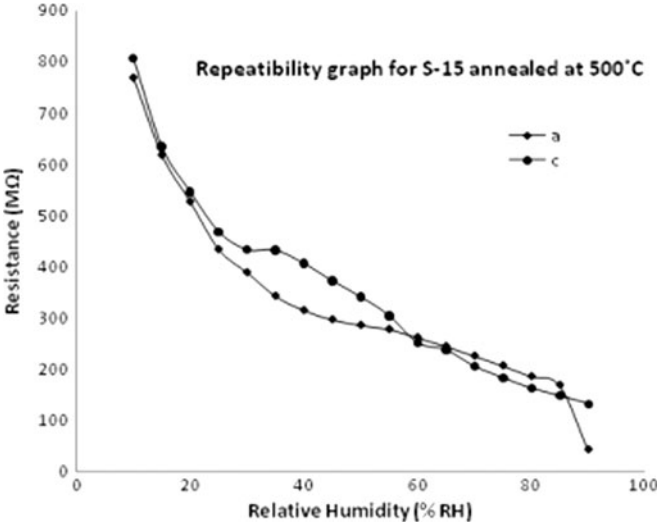

Figure 5. Variation of resistance with % RH for sensing element *S*-15 for annealing temperature, 500°C. a. increasing cycle; c. repeat cycle after six months.

the sensing elements are exposed leading to more adsorption of water molecules. This increases sensitivity of the sensing elements.

3.5 *Response and recovery times*

The measured response time of sensing elements *S*-10, *S*-15 and *S*-20 are found to be 125 s, 84 s and 119 s, respectively. The recovery time of sensing elements *S*-10, *S*-15 and *S*-20 are found to be 462 s, 396 s and 486 s, respectively. As compared to all this the measured response and recovery times of the sensing element of pure ZnO are 128 s and 452 s, respectively. Adsorption and desorption of the water molecules take place at different energy levels. Adsorption is an exothermic process, whereas desorption needs external energy for water molecules to depart from the metal oxide surface. Since desorption is an endothermic process, it takes a longer time to desorb water vapour; therefore, the recovery time is always greater than the response time (Sundaram *et al* 2004; Saha *et al* 2005).

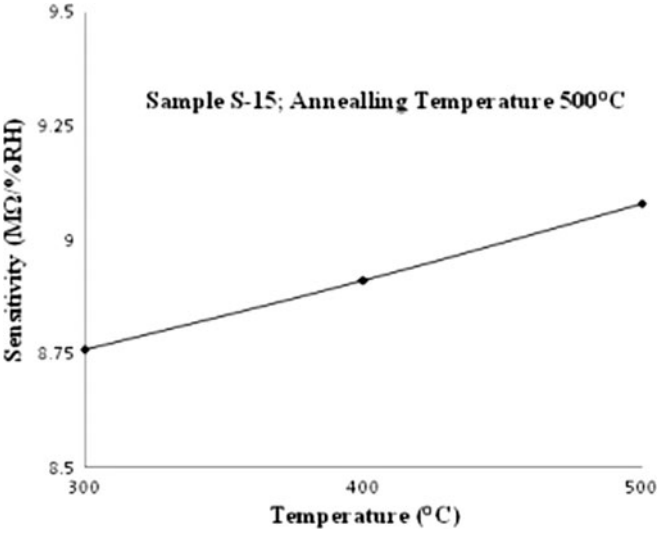

Figure 6. Variation of sensitivity with temperature for sensing element *S*-15 for annealing temperature, 500°C.

3.6 *Problem of ageing in humidity sensors*

Metal oxide sensors suffer from the problem of ageing. Ageing mechanisms in humidity sensors may be due either to prolonged exposure of surface to high humidity, adsorption of contaminants preferentially on the cation sites, loss of surface cations due to vapourization, solubility and diffusion, or annealing to a less reactive structure, migration of cations away from the surface due to thermal diffusion. Generally the more sensitive a material is to humidity, the more it tends to be susceptible to ageing. This is a significant problem in sensing devices (Kulwicki 1984; Shimizu *et al* 1985).

To see the effect of ageing, the sensing elements have again been exposed to humidity in the chamber after six months and variation of resistance with % RH recorded. Corresponding values of sensitivity after six months for these sensing elements are depicted in column **c** of table 1. Sensing element *S*-15 shows the best reproducible results. In figure 5 we present the repeatability graph for the best sensing element *S*-15. In this figure **a** represents initial increasing cycle of % RH and **c** represents increasing cycle after six months. It may be observed from table 1 that the repeatability in the value of sensitivity is within ±0·33% of the measured value after six months for sensing element *S*-15 whereas repeatability is within 1·29% for sensing element *S*-10 and a very high value of nearly 20% for *S*-20 for the annealing temperature of 500°C. The repeatability after six months for

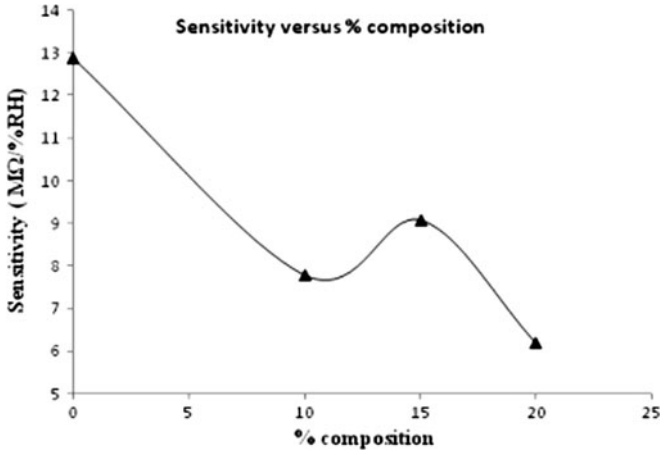

Figure 7. Variation of sensitivity with % composition for annealing temperature, 500°C.

the sensing element of pure ZnO for the annealing temperature of 500°C is high at 2·8%. Thus, sensing element *S*-15 shows good reproducibility and low hysteresis for annealing temperature of 500°C. Sensing element *S*-15 shows good reproducibility and lower hysteresis for annealing temperatures of 300°C and 400°C as well. However, the results of good sensitivity and very low hysteresis are best obtained for the sensing element annealed at 500°C. Figure 6 shows graph between sensitivity and annealing temperature for the sensing element *S*-15. It is seen that for sensing element *S*-15, the sensitivity increases with increase in the annealing temperature. Figure 7 shows the graph between the sensitivity and % weight of TiO_2 in ZnO for annealing temperature of 500°C.

4. Conclusions

As relative humidity increases, there is decrease in the resistance of pellets in the range 10 to 90% RH. Sensing element of pure ZnO shows higher sensitivity. When TiO_2 is added to ZnO, the overall sensitivity decreases. However, for the sensing element with 15 weight % of TiO_2 in ZnO having sensitivity of 9·08 MΩ/%RH in 10 to 90% relative humidity range, the reproducibility is the highest, well within 1% after six months. The hysteresis for this sensing element is the lowest of all, within 2%, which is comparable to the commercially available sensors. The response and recovery times of this sensing element are the lowest at 84 s and 396 s. Thus, the ZnO–15% TiO_2 nanocomposite sensor shows good sensitivity, least effect of ageing, lowest hysteresis, lowest response and recovery times; and is cheap and robust.

Acknowledgements

Authors would like to thank the University Grants Commission, New Delhi, for providing financial support for carrying out this research work [(File No. 33-23-2007 (SR)]. We would also like to thank the Geological Survey of India, Lucknow, for providing XRD and SEM facilities.

References

Dulin F H and Rase D E 1960 *J. Am. Ceram. Soc.* **43** 125
HIH-3605 humidity sensor data sheet (www.honeywell.com)
Huang M H, Wu Y, Feick H, Tran N, Weber E and Yang P 2001 *Adv. Mater.* **13** 113
Ivetic T, Nikolic V, Nikolic M, Blagojevic V, Duric T, Sreckovic M and Ristic M 2007 *Science of Sintering* **39** 153
Jayanti K, Chawla S, Sood K N, Chhibara M and Singh S 2009 *Appl. Surf. Sci.* **255** 5869
Kishimoto S, Yamamoto T and Nakagawa Y 2006 *Super Lattices Microstruct.* **39** 306
Kulwicki B M 1984 *J. Phys. Chem. Solids* **45** 1015
Lopatiuk O and Chernyak L 2005 *Appl. Phys. Lett.* **87** 214110
Margionte M A L, Simões A Z, Riccardi C S, Filho F M, Ries A, Perazolli L and Varela J A 2006 *Ceram. Int.* **32** 713
Ohbuchi Y, Kawahara T, Okamoto Y and Morimoto J 2001 *Jpn. J. Appl. Phys.* **40** 213
Pandey N K and Tiwari K 2010 *Sensor & Trans.* **122** 9
Pandey N K, Tripathi A, Tiwari K, Roy A, Rai A, Awasthi P, Mishra A and Kumar A 2008 *Sensor & Trans.* **96** 42
Pandey N K, Tripathi A, Tiwari K and Roy A 2009 *Adv. Mater. Res.* **79** 365
Pandey N K, Tiwari K and Roy A 2011 *IEEE Sensor J.* **11** 2142
Raid A, Ismail A, Al-Naimi Ala and Al-Ani Alaa A 2006 *J. Surf. Sci. Nanotech.* **4** 636
Reddy V B, Goel S P and Mehrotra P N 1984 *J. Mater. Chem. Phys.* **10** 365
Saha D, Giri R, Mistry K K and Sengupta K 2005 *Sensor Actuator B Chem.* **107** 323
Shimizu Y, Shimabukuro M, Arai H and Seiyama T 1985 *Chem. Lett.* **14** 917
Sundaram R, Raj Edwin S and Nagaraja K S 2004 *Sensor Actuator* **B99** 350
Thermoset Polymer-based Capacitive Sensors, Application Sheet (www.honeywell.com)
Traversa E 1995 *Sensor Actuator* **B23** 135
Xia Y, Yang P, Sun Y, Wu Y, Mayers B, Gates B, Yin Y, Kim F and Yan H 2003 *Adv. Mater.* **15** 353
Yadav B C, Pandey N K, Srivastava A and Sharma P 2007 *J. Meas. Sci. Technol.* **18** 260
Yarkin D G 2003 *Sensor Actuator* **107** 1
Yavale S P, Yavale S S and Lamdhade G T 2007 *Sensor Actuator* **A135** 388
Yildiz K, Karakus N, Toplan N and Toplan H O 2007 *Mater. Sci. Poland* **25** 1135
Yogeeswaran G, Chenthamarakshan C R, Tacconi N R and Rajeshwar K 2006 *Mater. Res. Soc.* **21** 3234